

# Modeling of Perception and Control of Attitude with Perspective Displays

Barbara T. Sweet\* and Mary K. Kaiser.†  
 NASA Ames Research Center, Moffett Field, CA, 94087

Pilots rely upon visual information conveyed by computer-generated perspective displays in cockpits, and also by out-the-window (OTW) scenes rendered in simulators, to perform control tasks. Because even the most advanced graphics system cannot recreate the full complexity of a natural perspective scene (due to limitations in spatial and temporal resolution, dynamic range, field-of-view, and scene detail), it is necessary to understand which characteristics of the perspective scene are used by the pilot to accomplish vehicular control. In the current study we investigated the effects of simulated OTW visual scene content on an operator's ability to control pitch attitude of a simulated vehicle in the presence of both pitch disturbances and longitudinal position disturbances. Two types of vehicle dynamics were simulated, first-order and second-order; two types of ground textures were assessed, and the task was performed with and without a visible horizon. Data from 12 participants were analyzed to determine task performance, and to estimate describing functions of the human operator characteristics. Task performance with both types of vehicle dynamics was significantly better with a visible horizon. The type of ground texture did not affect performance. Parameterized models were fit to the describing function measurements. The resulting models exhibited excellent correlation with the describing functions. Identified parameters related to the visual cue usage showed excellent correlation with the available scene features.

## Nomenclature

$\theta$	= pitch attitude, radians
$\delta$	= operator control output, dimensionless (range from -1.0 to 1.0)
$x$	= longitudinal position, eyeheights
$H_x$	= model, operator control output to longitudinal position input
$\hat{H}_x$	= describing function measurement, operator control output to pitch attitude input
$H_\theta$	= model, operator control output to longitudinal position input
$\hat{H}_\theta$	= describing function measurement, operator control output to pitch attitude input
$K_X$	= visual cue weighting parameter for longitudinal position, rad/eyeheight
$RMS()$	= root mean square
$P(\theta)$	= percentage of control energy correlated with pitch attitude disturbance
$P(x)$	= percentage of control energy correlated with longitudinal disturbance
$L$	= objective function for model fitting
$K_P$	= gain parameter, $H_\theta$ model, control units/rad
$\tau$	= time delay parameter, $H_\theta$ model, seconds
$\omega_N$	= neuromuscular natural frequency, $H_\theta$ model, rad/sec
$\zeta_N$	= neuromuscular damping ratio, $H_\theta$ model
$\tau_L$	= lead time constant, $H_\theta$ model, seconds
$\omega_C$	= crossover frequency, rad/sec
$\phi_M$	= phase margin, degrees

\* Aerospace Engineer, Human Information Processing Research Branch, MS 262-2, Professional Member AIAA.

† Research Psychologist, Human Information Processing Research Branch, MS 262-2.

$\phi_{\delta U}$	=	cross spectral density, control and pitch attitude disturbance, control units*rad
$\phi_{\theta U}$	=	cross spectral density, control and pitch attitude disturbance, rad <sup>2</sup>
$\phi_{\delta X}$	=	cross spectral density, control and longitudinal position disturbance, control units*eyeheights
$\phi_{XX}$	=	power spectral density, pitch attitude disturbance, eyeheights <sup>2</sup>

## I. Introduction

THIS paper describes a modeling technique that accounts for perspective scene viewing during closed-loop manual control of pitch attitude. Two of the prominent models of manual control are the crossover model<sup>1</sup> and the optimal control model<sup>2</sup>. Manual control models, however, have been primarily developed using compensatory and pursuit<sup>‡</sup> displays, as opposed to perspective displays.

Several researchers have extended the manual control methodologies by combining the optimal control model of the human operator with models of perspective-scene viewing. Grunwald and his colleagues have studied manual control extensively using perspective scenes for a variety of tasks and display types<sup>3-12</sup>. Zacharias developed general models of perspective-scene viewing using optimal control models<sup>13,14</sup>, which have been applied to the analysis and design of simulator visual cues<sup>15,16</sup>. Wewerinke applied optimal control modeling techniques to examine the visual cues necessary for glideslope control in the landing task<sup>17,18</sup>.

Other researchers have used the crossover model to characterize manual control with perspective scene viewing. Johnson and Phatak<sup>19</sup> showed that the crossover model, coupled with a simple representation of a scene feature, accurately described the actions of a pilot performing an altitude control task. Mulder examined variations in identified crossover model parameters resulting from variations in the design of a tunnel-in-the-sky display, but did not directly model the perspective scene characteristics<sup>20</sup>. One of the authors of this paper used a combination of the crossover model with a model of perspective scene viewing to describe the operators characteristics when controlling longitudinal position with a perspective scene<sup>21,22,23</sup>. In that study, operators were instructed to maintain a fixed longitudinal position in the presence of disturbances in both pitch and longitudinal position (the operator could only control longitudinal position, not pitch attitude). The results suggested that certain features in the perspective scene, particularly lines-of-splay<sup>§</sup>, were beneficial to task performance. Another interesting finding was that operators appeared to use two independent sources of information in the scene to obtain position and velocity information.

For the study described in this paper, the control paradigm of the previous study is reversed; the operator is required to control pitch attitude in the presence of both pitch and longitudinal position disturbances. In Section II, the methodology for describing function measurement and scene perception modeling will be described; Section III contains a description of the experimental method and results; these results are discussed in Section IV. Finally conclusions are presented in Section V.

## II. Modeling Methodologies

This section describes the methods used to represent perspective display perception in manual control models, methods to relate modeling parameters to perspective scene features, and methods to identify describing functions of the human operator.

### A. Perspective Scene Perception

An operator controlling with a compensatory display is receiving direct information about the vehicle state error. In the case of perspective-scene viewing, the operator must rely indirectly on features and cues in the display to derive information about the controlled state. Sometimes, a feature or cue can be perfectly correlated with the vehicle state being controlled. However, frequently there are no cues in the display that isolate the variable of interest; vehicle states become coupled through the perspective transformations. The pitch-control task serves as an example. When the horizon is visible, the elevation of the horizon in the display is perfectly correlated with pitch attitude, and is not in any way affected by longitudinal position changes. However, when the horizon is obscured, as with fog, the situation changes. The location of the visible features in the display are then affected by both pitch attitude and longitudinal position.

---

<sup>‡</sup> In a compensatory display, only the error between the current state and target state is presented to the operator. In a pursuit display, both the current state and target state are presented to the operator.

<sup>§</sup> Lines-of-splay are formed by linear scene features parallel to the direction of motion.

The mathematical relationship between vehicle states and perspective scene features can be complex and nonlinear. The method commonly employed, in both the crossover and optimal control techniques, is to linearize the perspective transformation process, allowing visual cues to be represented as a linear combination of the vehicle states. More detailed treatments of this method are available in the previously referenced literature. For the purposes of this experiment, we will simply define a visual cue ( $\gamma$ ) used by the operator to control pitch attitude, as a linear combination of pitch attitude ( $\theta$ ) and longitudinal position ( $x$ ):

$$\gamma = \theta + K_X x \quad (1)$$

An example relating the weighting factor  $K_X$  to a particular perspective scene feature follows.

### B. Visual Cue Characteristics

To relate the  $K_X$  weighting factor to the visual display, it is necessary to first define a potential visual cue, and then develop an expression that relates the cue to the vehicle states. One very likely cue in this case is the vertical location, in the display, of a feature on the ground. We define  $D_X$  as the longitudinal displacement of a ground feature (in a ground-fixed reference system), and  $x$  and  $\theta$  as the longitudinal position and pitch attitude of the vehicle. The expression that relates the vertical location,  $z$ , of the feature in the display, is (see Reference 22):

$$z = -F \frac{((D_X - x) \sin(\theta) + \cos(\theta))}{((D_X - x) \cos(\theta) - \sin(\theta))} \quad (2)$$

where  $F$  is the focal length of the imaging device. Taking the differential of this cue yields:

$$dz = \frac{\partial z}{\partial x} dx + \frac{\partial z}{\partial \theta} d\theta \quad (3)$$

Lastly, a linearized visual cue can be defined by evaluating this expression at  $x=0$ ,  $\theta = 0$ :

$$dz = \left( \frac{\partial z}{\partial x} \Big|_{x=0, \theta=0} \right) x + \left( \frac{\partial z}{\partial \theta} \Big|_{x=0, \theta=0} \right) \theta \quad (4)$$

We define the visual cue for incorporation in the model as proportional to  $dz$ , such that the gain on the controlled state,  $\theta$ , is equal to unity\*\*:

$$dz \propto \gamma = \theta + \frac{(\partial z / \partial x) \Big|_{x=0, \theta=0}}{(\partial z / \partial \theta) \Big|_{x=0, \theta=0}} x \quad (5)$$

We will now substitute  $dx = x$ ,  $d\theta = \theta$ , understanding that this expression is only valid for small displacements in  $x$  and  $q$ . Evaluating the partial derivatives will yield the following expression:

---

\*\* While this is not a requirement for the definition of any visual cue, normalization of the cue to the controlled state aids in interpretation of the modeling parameters. Independent weights for  $\theta$  and  $x$  would result in an ambiguity in the interpretation of the weighting on pitch and gain in the operator describing function.

$$\gamma = \theta + \frac{-F/D_x^2}{-F\left[1 + \frac{1}{D_x^2}\right]} x = \theta + \frac{1}{(D_x^2 + 1)} x \quad (6)$$

The relationship between the position of a visual feature and the weight in the visual cue definition is:

$$K_x = \frac{1}{(D_x^2 + 1)} \quad (7)$$

This represents an important relationship that will be used to relate identified parameters for  $K_X$  to the perspective scene features.

### C. Describing Function Measurements

A block diagram depicting the experimental paradigm is shown in Fig. 1.  $Y_C$  represents the controlled element dynamics (first- or second-order),  $Y_P$  represents the human operator,  $\delta$  is the control output of the human operator, and  $\gamma$  is the visual cue the operator is using. With proper design of the disturbance signals  $u$  and  $x$ , the describing functions can be estimated from cross- and power-spectral densities<sup>24,25</sup>:

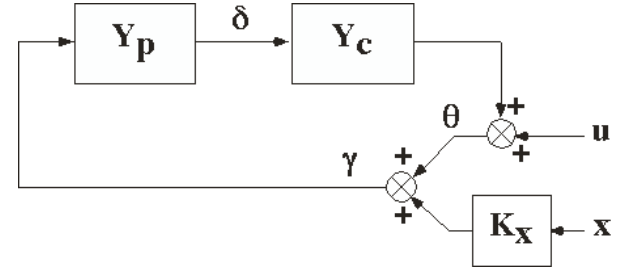


**Figure 1. Conceptual block diagram of human operator ( $Y_P$ ) performing closed-loop control using a visual cue ( $\gamma$ ) as input.**

$$\hat{H}_\theta \approx \frac{\phi_{\delta U}}{\phi_{\theta U}} \quad (8)$$

$$\hat{H}_X \approx \frac{\phi_{\delta X}}{\phi_{X X}} \quad (9)$$

These describing function measurements are related to the components in Figure 1 as follows:

$$H_\theta = Y_P \quad (10)$$

$$H_X = \frac{Y_P K_X}{(1 + Y_P Y_C)} \quad (11)$$

Our goal in this experiment will be to relate the describing function estimates to the system components in Fig. 1 and, more specifically, to relate identified values of  $K_X$  to the perspective scene features.

## III. Experiment Description

### A. Method

#### 1. Participants

Twelve male, general-aviation pilots participated in the study. They were recruited from a paid contractor pool at Ames Research Center. The subjects had on average 1154 hours of flying experience; all of the subjects had pilot certificates in fixed-wing aircraft; none had experience in helicopters. Ten participants reported being right-handed, one reported left-handed, and one reported ambidextrous.

## 2. Apparatus

The experimental control program was run on a Silicon Graphics Octane 2 computer. Control inputs were made via a B&G Systems JF3 3-axis joystick (only the longitudinal degree of freedom of the stick was active; the lateral and yaw inputs were disabled). The control and display were refreshed at a rate of 60 Hz. The color monitor had a 20-inch diagonal screen, with a resolution of 1280 (horizontal) by 1024 (vertical) pixels. The participants were seated approximately 20 inches from the display, resulting in subtended visual angles of approximately 37.5° horizontal by 30° vertical.

## 3. Stimuli and Control Tasks

The displays were rendered with a 75° by 60° (horizontal by vertical) viewing frustum. Hence, given the viewing geometry, the displays presented a 2X minification. All of the display conditions presented a green ground plane below the operator. In half of the conditions, the horizon formed by the ground plane and sky was visible; in the other half, the horizon was obscured by fog. In the visible-horizon displays, a vertical segment was added to the end of the ground plane (at a distance of 20 eye-heights) to mimic the appearance of a true horizon. In the cases where the horizon was obscured, we utilized a combination of the fog function in OpenGL<sup>26</sup>, and Gouraud (smooth) shading of the ground-plane polygon and texture elements to match the fog color.

The ground texture was rendered as a large number of individual diamond-shaped polygons. These were rendered in two different ways; in one condition (unaligned texture), the orientation of the diamonds was random; in the other condition (aligned texture), the diamonds were oriented with their long axis parallel to the direction of longitudinal motion. The displays with the visible horizon are shown in Figs. 2(a) and 2(b); the displays with fog obscuring the horizon are shown in Figs. 2(c) and 2(d).

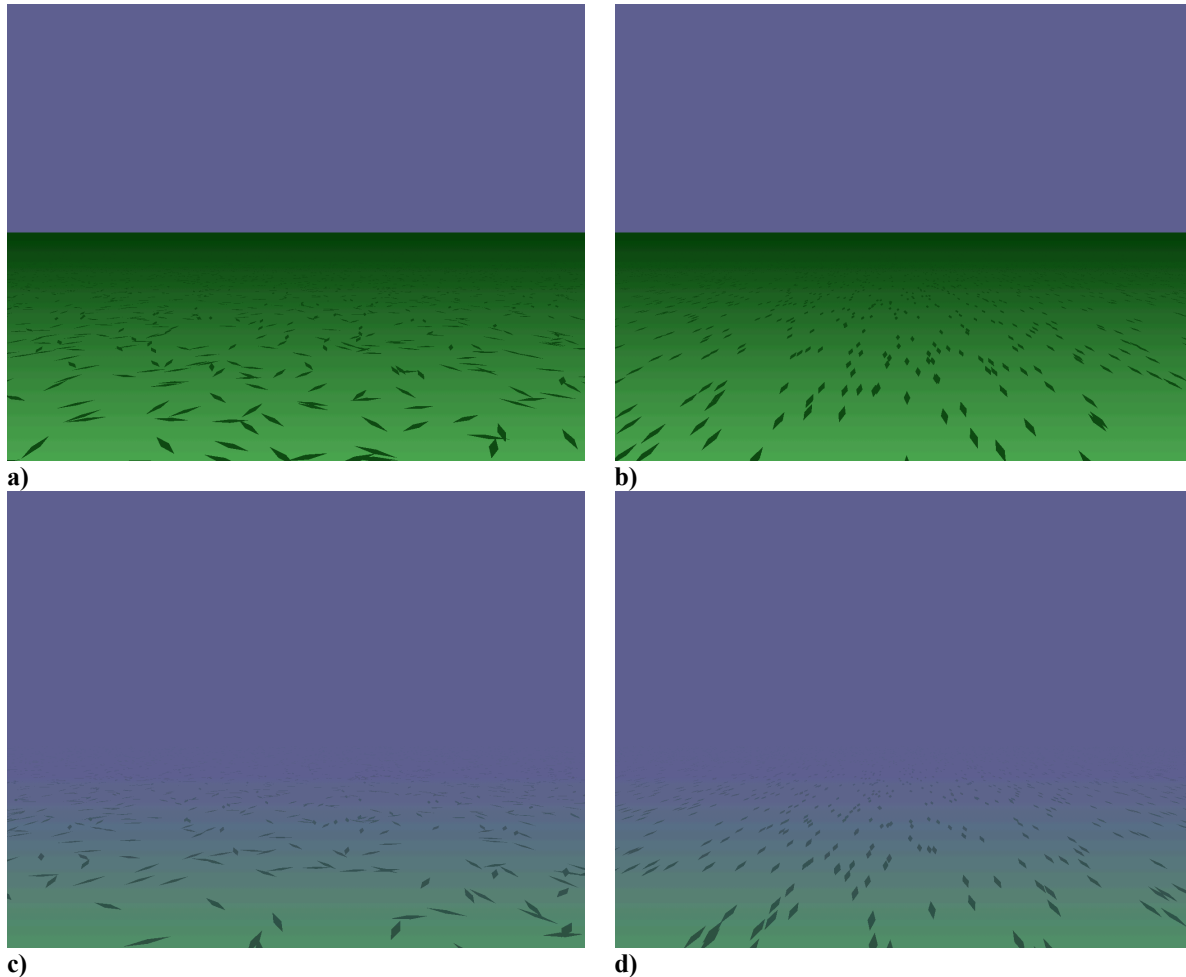


**Figure 1. Scene displays. Visible horizon and unaligned texture (a), visible horizon and aligned texture (b), non-visible horizon and unaligned texture (c), non-visible horizon and aligned texture (d).**

The only degrees of freedom of the “vehicle” were pitch attitude and longitudinal position. The operator was able to control the pitch attitude only; the longitudinal position was not controlled by the operator. The experimental task was to maintain a constant (zero) pitch attitude in the presence of apparently random disturbances. Both pitch rate and longitudinal position were perturbed by sum-of-sines disturbances; the disturbances were designed to be spectrally independent to facilitate describing function measurement. All other vehicle states remained constant. The altitude of the operator's viewpoint was defined to be 1.0 eyeheight and was adopted as the measuring unit for longitudinal position. Two types of controlled element dynamics were tested: first-order and second-order. Detailed descriptions of the controlled element dynamics and disturbances are provided in the Appendix.

#### 4. Procedure

Participants were informed of the nature of the study, and received written instructions. The experiment was largely self-paced. Each pilot participated in the experiment on two consecutive days. Only one type of controlled element dynamics (first- or second-order) was presented on a given day, with the order of presentation counterbalanced across participants.

Participants completed four experimental conditions each day (texture aligned vs. unaligned crossed with horizon visible vs. obscured). Prior to the experimental sessions, participants received five one-minute training runs in the four conditions they would encounter that day. Participants were specifically instructed to use these training runs to develop their control strategies, and to maintain a consistent strategy in all of the experimental sessions of that condition. The data runs were conducted in blocks of four, ~4-minute sessions for each condition, one in the morning and one in the afternoon, for a total of eight data runs per condition. Participants were encouraged to rest between sessions, and were required to take breaks between blocks.

## B. Results

### 1. Statistical Analyses

Five dependent measures were considered; three of the dependent measures were root mean square (*RMS*) values of pitch attitude ( $RMS(\theta)$ ), pitch rate ( $RMS(d\theta/dt)$ ), and operator control outputs ( $RMS(\delta)$ ). The two additional dependent measures were based on the control power correlation with the input disturbances: percent of control power correlated with the pitch disturbance ( $P(\theta)$ ) and percent of control power correlated with the longitudinal disturbance ( $P(x)$ ). A 2x2x2 (control task x horizon visibility x texture) repeated-measures ANOVA was performed. For pitch attitude RMS (Fig. 3a), there were significant main effects for control task ( $F[1,11] = 67.9, p < 0.0005$ ) and horizon condition ( $F[1,11] = 39.05, p < 0.0005$ ); pilots maintained pitch significantly better with the first-order control task and with a visible horizon. Similarly, pitch rate RMS (Fig. 3b) was significantly lower with the first-order control task ( $F[1,11] = 18.8, p < 0.001$ ) and with a visible horizon ( $F[1,11] = 6.66, p < 0.03$ ).

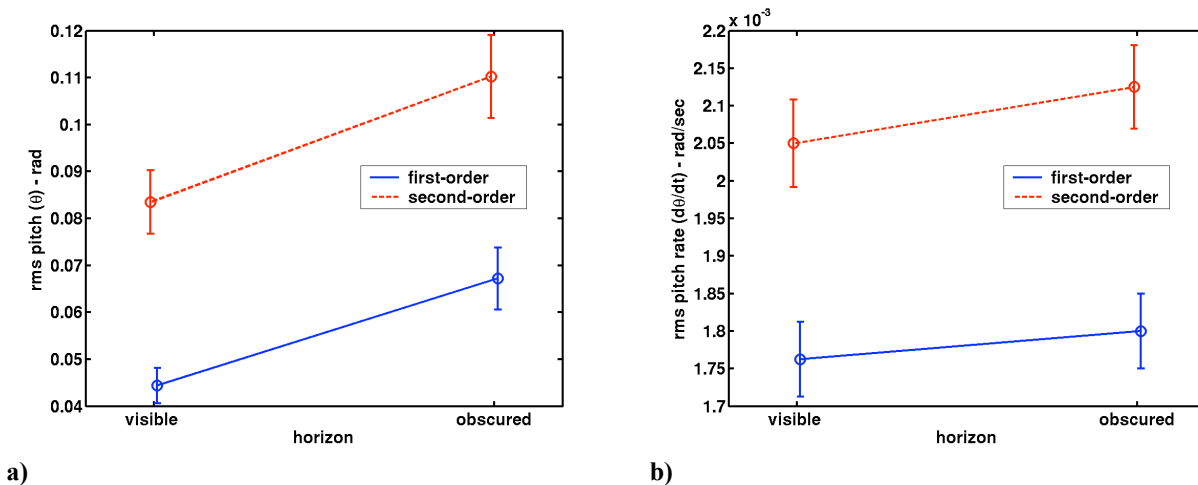


Figure 3. Mean and standard errors of pitch attitude RMS (a) and pitch rate RMS (b).

For operator control output (Fig. 4), RMS was significantly smaller for the first-order control task ( $F[1,11] = 74.7, p < 0.0005$ ). The percent of control correlated with the pitch attitude disturbance (Fig. 5a) was likewise significantly greater with the first-order control task ( $F[1,11] = 27.9, p < 0.0005$ ), and with a visible horizon ( $F[1,11] = 23.94, p < 0.0005$ ). The percent of control activity correlated with the longitudinal position disturbance (Fig. 5b) was significantly affected only by horizon visibility ( $F[1,11] = 9.104, p < 0.02$ ).

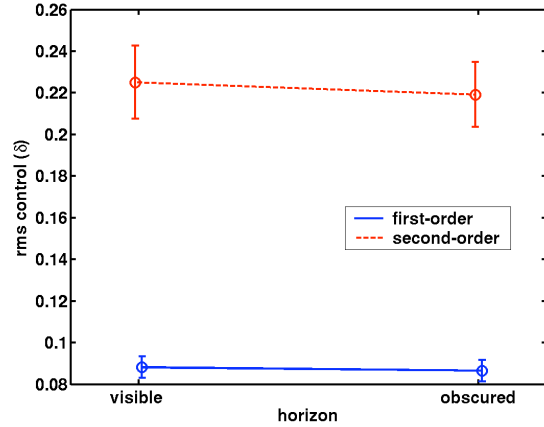
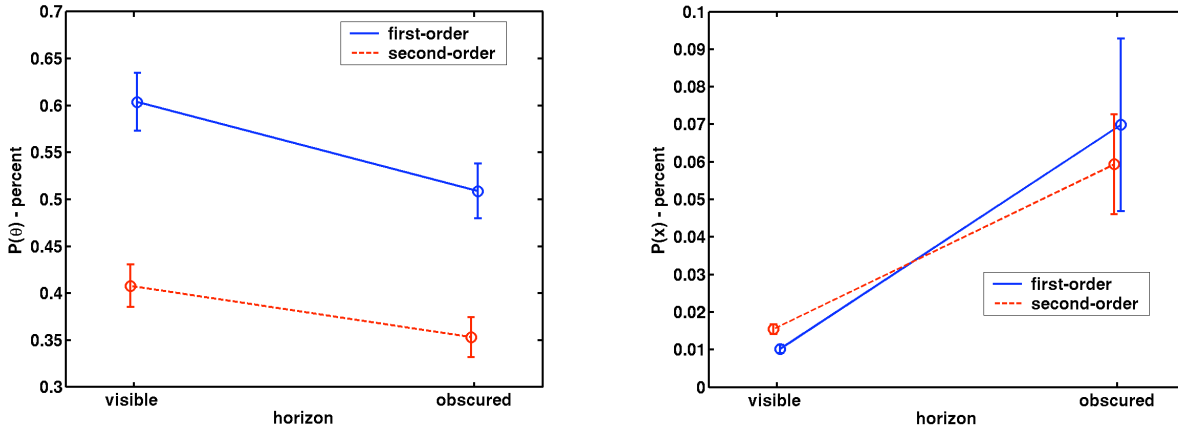


Figure 4. Mean and standard errors of control RMS.



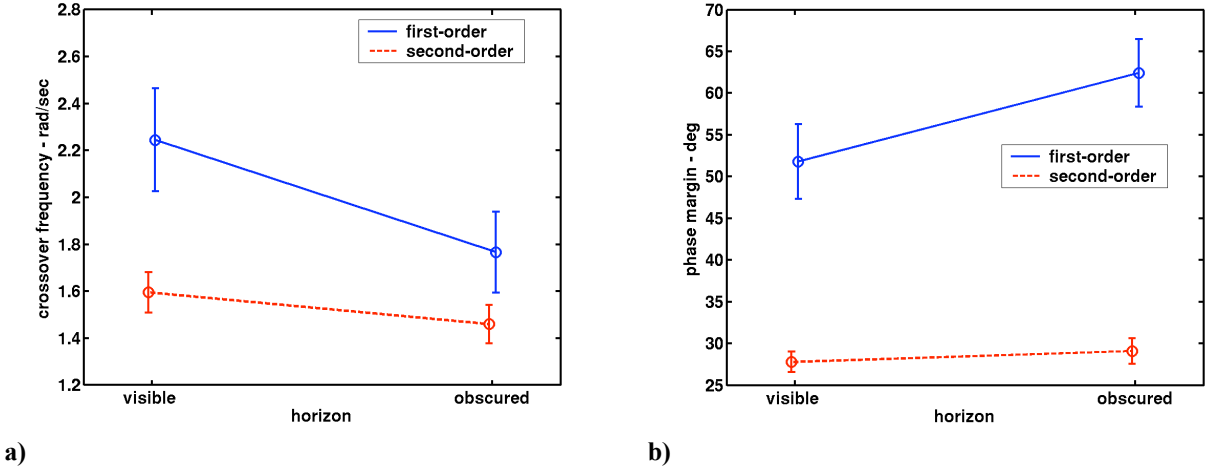
a) Figure 5. Mean and standard errors of the percent of control correlated with pitch attitude disturbance ( $P(\theta)$ , (a)), and longitudinal position disturbance ( $P(x)$ , (b)).

## 2. Describing Function

Describing functions were estimated from the time histories of the control ( $\delta$ ), pitch attitude ( $\theta$ ), longitudinal position ( $x$ ), and pitch attitude disturbance ( $u$ ), as described in Section IIC. Two describing functions were estimated:  $\hat{H}_\theta$ , the relationship between the operator's control output and pitch attitude, and  $\hat{H}_x$ , the relationship between the operator's control output and longitudinal position. Seven of the eight data runs in each condition were used for the describing function estimate; the data run with the greatest pitch attitude RMS was omitted<sup>††</sup>. Crossover frequencies ( $\omega_c$ ) and phase margins ( $\phi_M$ ) were determined from the product of the describing function for pitch and the controlled element dynamics ( $\hat{H}_\theta Y_c$ ); see Fig. 6. A 2x2x2 (control task x horizon visibility x texture) repeated-measures ANOVA was performed. For crossover frequency (Fig. 6a), there were main effects for control task ( $F[1,11] = 11.44, p < 0.01$ ) and horizon visibility ( $F[1,11] = 15.374, p < 0.005$ ); crossover frequency was greater for the first-order control task, and was reduced when the horizon was obscured. There was also an interaction between control task and horizon visibility ( $F[1,11] = 6.84, p < 0.03$ ); the decrease in crossover frequency with the obscured horizon was greater for the first-order control task than for the second-order control task. A complementary pattern was observed with phase margin (Fig. 6b); there were main effects for control task ( $F[1,11] = 68.72, p < 0.0005$ ) and horizon visibility ( $F[1,11] = 14.35, p < 0.005$ ), and an interaction between control

<sup>††</sup> The choice to eliminate one data run was made to exclude data with extremely large excursions in pitch (i.e., complete 360° pitch rotation). Two participants did this, each for only one run in one condition.

task and fog condition ( $F[1,11] = 11.84, p < 0.01$ ). Phase margin was greater for first-order control; it was also greater for the obscured horizon, but primarily within the first-order control condition.



a) **Figure 6. Mean and standard errors of crossover frequency (a) and phase margin (b) of operator-controlled element describing function.**

### 3. Modeling

Parameterized models were developed for the describing functions. Although the operator is controlling based upon the information contained in the perspective scene, it is reasonable to assume the operator finds features in the scene that correlate highly with the variable to be controlled. Therefore, a describing function form similar to one expected with a conformal pitch display would be appropriate. For the pitch describing function,  $H_\theta$ , the following parameterized model form was used:

$$H_\theta(s) = -\frac{K_P \exp(-s\tau)(s\tau_L + 1.0)}{(s^2/\omega_N^2 + 2s\zeta_N/\omega_N + 1.0)} \quad (12)$$

This model is a simplification of the precision model extension of the crossover model<sup>1</sup>.  $K_P$  is a gain,  $\tau$  is a time delay,  $\tau_L$  is the time constant of a lead term, and  $\omega_N$  and  $\zeta_N$  are the natural frequency and damping of a second-order neuromuscular dynamics term. Addition of another neuromuscular dynamic lag term (present in the precision model) did not improve the quality of model fits. Because a relatively large number of the describing function measurements were excessively noisy at low frequency, the lowest two frequencies were not used for model fitting; because of this, a low-frequency lead-lag term in the precision model was also not incorporated.

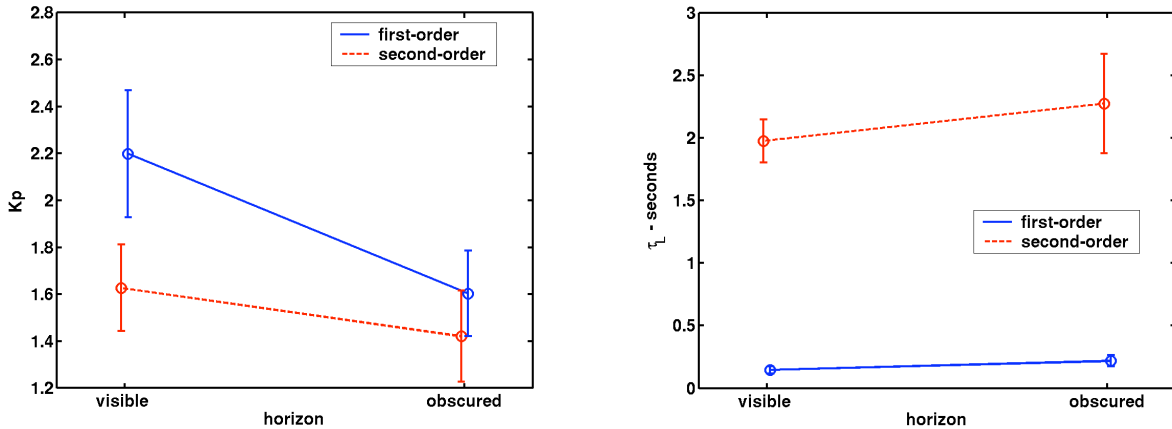
The model parameters were chosen to minimize the objective function:

$$L(H, \hat{H}) = \sum_{i=1}^N \left\{ \frac{\text{real}(H(j\omega_i) - \hat{H}(j\omega_i))^2}{\text{se}(\text{real}(\hat{H}(j\omega_i)))^2} + \frac{\text{imag}(H(j\omega_i) - \hat{H}(j\omega_i))^2}{\text{se}(\text{imag}(\hat{H}(j\omega_i)))^2} \right\} \quad (13)$$

where  $H$  is the parameterized model, and  $\hat{H}$  is the describing function measurement. The term  $\text{se}()$  is the estimate of the standard error of the describing function, based on seven samples.

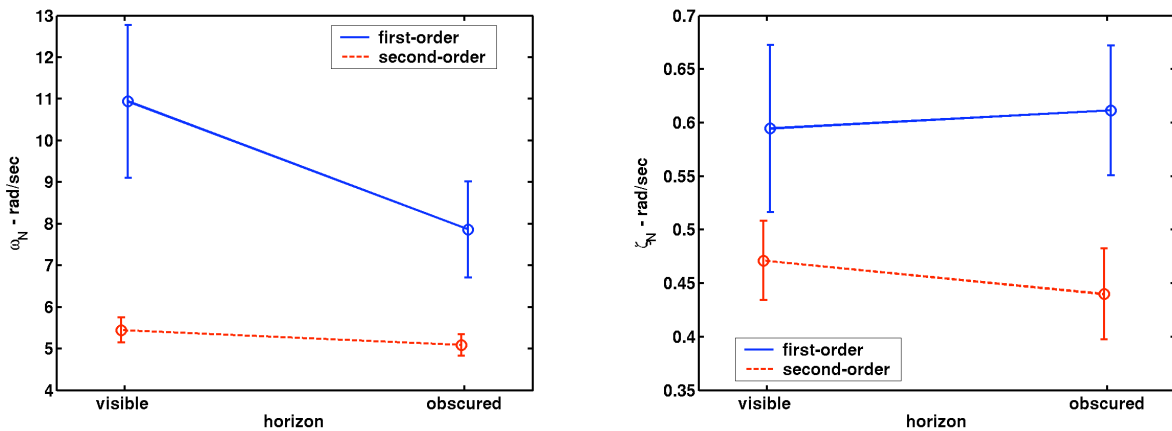
Independent 2x2x2 (control task x horizon visibility x texture) repeated-measures ANOVAs were performed on the five parameters resulting from the model fit. The gain term  $K_P$  (Fig. 7a), was significantly larger when the horizon was visible ( $F[1,11] = 18.6, p < 0.005$ ). The apparent trend towards a larger gain with the first-order control task was not statistically significant ( $F[1,11] = 3.63, p > 0.05$ ). There were no main effects for the time delay term  $\tau$  which averaged .264 seconds across conditions. The lead time constant  $\tau_L$  (Fig. 7b) demonstrated a main effect for control task ( $F[1,11] = 53.35, p < 0.0005$ ): the first-order task,  $\tau_L$  averaged .182 seconds with a standard

error of .035 seconds<sup>‡‡</sup>, while the second-order task averaged 2.125 seconds with a standard error of .263 seconds. The neuromuscular natural frequency  $\omega_N$  (Fig. 8a) was significantly higher with first-order control dynamics ( $F[1,11] = 10.788$ ,  $p < 0.01$ ) and with a visible horizon ( $F[1,11] = 6.83$ ,  $p < 0.03$ ); the apparent trend towards an interaction between control task and horizon visibility was not significant ( $F[1,11] = 4.19$ ,  $p > 0.05$ ). The neuromuscular damping  $\zeta_N$  (Fig. 8b) demonstrated a main effect of control task ( $F[1,11] = 5.56$ ,  $p < 0.05$ ), with greater damping associated with first-order control.



a) **Figure 7. Mean and standard errors of human operator gain  $K_p$  (a) and lead time constant  $\tau_L$  (b).**

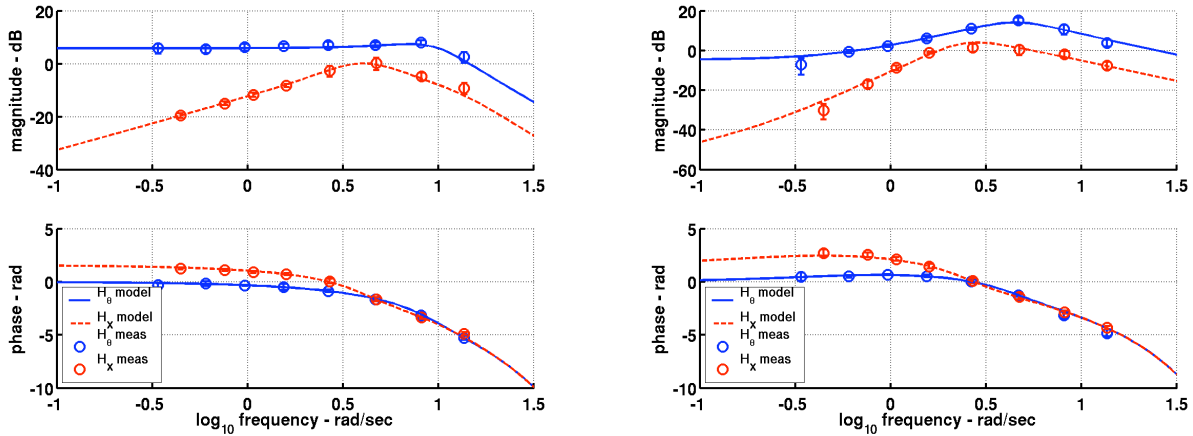
Overall, the correspondence between the models and measurements was quite good; the error between the model and measurement had an average magnitude of .03 dB, with a standard deviation of 1.7 dB, and a mean angle of 1.3 degrees with a standard deviation of 11.5 degrees.



a) **Figure 8. Mean and standard errors of neuromuscular natural frequency  $\omega_N$  (a) and neuromuscular damping  $\zeta_N$  (b).**

For the conditions with the horizon visible, the low amount of control activity associated with the longitudinal position made it impossible to estimate describing functions to longitudinal position,  $\hat{H}_X$ . However, this describing function was estimated for all of the conditions with the horizon obscured, and the weight  $K_X$  was estimated for all operators and available conditions. Figure 9 shows an example of the fitted model and measurements.

<sup>‡‡</sup> Although the crossover model does not predict that a lead term is necessary in first-order control, this modest amount of lead significantly improved the model fit, reducing the objective function an average of 31%.



a) **Figure 9. Example plot of describing function measurements and model fits, for first-order (a) and second-order (b) control task and the aligned texture display with the horizon obscured. 95% confidence intervals are shown on the measurements. With seven repetitions of each condition being used to form the describing function estimates, relatively small confidence intervals are typical. For the first-order case,  $K_X = 0.234$ , for second-order,  $K_X = 0.218$ .**

For the visual scenes in which the horizon is obscured, features are visible in a limited portion of the display. The features at the bottom of the display are the most visible, both because of their greater visual size and higher contrast. For a 60-degree vertical field of view, the location (in the world) of a feature at the bottom of the display would be  $D_X = 1/\tan(30^\circ)$ , or  $D_X = 1.732$  eyeheights. For a feature at the limit of sufficient visual contrast ( $\sim 15^\circ$  below the horizon), the location of the feature (in the world) would be  $D_X = 1/\tan(15^\circ)$ , or  $D_X = 3.73$  eyeheights. From Eq. 7, this would result in values of  $K_X$  ranging from 0.25 (at the bottom edge of the display) to 0.067 (the approximate limit of sufficient contrast at  $\sim 15^\circ$ ). Note that the identified values of  $K_X$  for the example plots shown in Fig. 9 are within this range (0.234 and 0.218). In fact, the identified values of  $K_X$  were almost completely within these boundaries, with a mean of 0.083 and standard error of 0.017. A 2x2 (texture x control task) repeated-measures ANOVA did not identify any main effects or significant interactions.

We can determine what vertical location in the display a particular value of  $K_X$  corresponds to using Eqs. (2) and (7). Fig. 10 shows the vertical position in the display corresponding to the identified  $K_X$  values, for each operator. Note that the lateral position in the figure specifies the operator and is *not* related to  $K_X$  - this was done to allow examination of the individual differences between the operators.

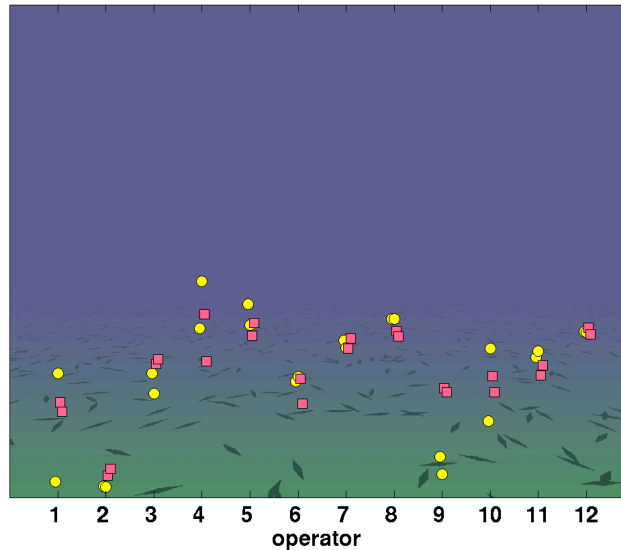


**Figure 10. Vertical locations in display predicted by identified values of  $K_X$ . Yellow circles correspond to the first-order task, pink squares correspond to the second-order task. There were no significant differences in the  $K_X$  values as a function of control task or texture.**

## IV. Discussion

Pitch attitude stabilization performance was better with a visible horizon than with the horizon obscured. This finding, coupled with the fact that very little of the control power was correlated with the longitudinal position disturbance when the horizon was visible, suggests that operators were capable of disregarding the position changes while controlling pitch attitude. When the horizon was obscured, both pitch attitude and pitch rate RMS increased relative to when the horizon was visible. Similarly, the percent of control power correlated with the pitch attitude disturbance decreased when the horizon was obscured, while the percent of control power correlated with the longitudinal disturbance by increased a similar amount. When the horizon is obscured, a component of the control output of the operator is in response to the longitudinal position disturbance; the operator is effectively injecting noise into the closed-loop system. Thus, a visible horizon prevents this source of noise.

The describing function measurements exhibited crossover frequency and phase margin characteristics as a function of control task, consistent with other manual control findings. Both crossover frequencies and phase margins were reduced with the second-order control task. There was also an interaction between control task and horizon visibility for both measures. When the horizon was obscured, crossover frequency decreased and phase margin increased with the first-order task, while the second-order task demonstrated little change associated with horizon visibility. This reduction in crossover frequency and increase in phase margin appear to be crossover regression, which is typically observed when the bandwidth of the input (or in this case, the disturbance) is increased. Obscuration of the horizon could create a perception of increased disturbance bandwidth because of greater reliance on cues that are affected by longitudinal position, but it is not clear why this effect is more evident with the first-order task than the second-order task.

The parameterized models exhibited a very good fit to the describing function measurements. Many of the model parameters exhibited characteristics that were consistent with the changes in the performance measures. The gain term  $K_P$  was lower when the horizon was obscured for both control tasks. This is consistent with the performance changes in pitch attitude and pitch rate RMS due to the visibility of the horizon. The lead time constant showed no effect from the horizon visibility; not surprisingly, the lead time constant was much higher in the second-order control task. There were some interesting results from the neuromuscular natural frequency,  $\omega_N$ . First,  $\omega_N$  was much lower in the second-order control task than the first-order, in the range of 5.0 to 6.0 rad/sec. Neuromuscular frequencies this low are typically the result of a pulsive (rather than continuous) control strategy<sup>28</sup>. There was also a trend towards an interaction between control task and horizon visibility; the neuromuscular natural frequency decreased somewhat in the first-order task, compared to no change in the second-order task. The mechanism behind this result is not yet known, and is the subject of further investigation.

The two texture conditions were tested to determine if line-of-splay visual features would help the operator disambiguate the effects of longitudinal position from the effects of pitch attitude. In the previous longitudinal control study<sup>21,22,23</sup>, lines-of-splay appeared to improve performance; in the current study, no significant effects for texture configuration were found. Lines-of-splay may play a greater role in the detection of position changes than in rejecting such displacements as an irrelevant cue.

The weighting parameter on longitudinal position,  $K_X$ , was identified for all of the conditions with the horizon obscured. The range of identified parameters, for all of the operators and both texture conditions, was relatively consistent with the proposed visual cue (i.e. vertical location of a feature in the display). The fact that the operators in the study typically did not achieve  $K_X$  lower than those expected using this visual cue suggests that the operators could not find a cue with better qualities (i.e. less influenced by longitudinal position).

## V. Conclusions

Explicit modeling of closed-loop manual control with perspective scene use can yield insights into how humans process out-the-window scene information to accomplish vehicle control. For the task described in this paper, human operator modeling, based upon the crossover model, provided fits to the measured describing function that were highly accurate. An additional model parameter, which represented visual cue selection and use, was highly consistent with the visual cue hypothesized for the scenes presented.

## Appendix

The controlled element dynamics and the disturbance characteristics are defined here. The longitudinal position  $x$  is expressed in eye heights, and displayed pitch attitude  $\theta$  is in radians. The control output of the operator  $\delta$  is in the range between  $-1$  to  $1$  (stick displacement). The longitudinal and pitch disturbances are represented by  $x$  and  $u$ , respectively. Fig. 1 contains a block diagram of the system.

For the first-order task, the controlled element was a single integrator:

$$Y_C(s) = \frac{1}{s} \quad (A1)$$

For the second-order task, the controlled element was a double intergrator:

$$Y_C(s) = \frac{1}{s^2} \quad (A2)$$

Both the longitudinal and pitch disturbances were based on a sum of 10 sines with unique frequencies for each degree-of-freedom. The individual frequencies were chosen to be multiples of the period established by the total run length (in this case, 240 seconds). This is accomplished by specifying discrete values of frequencies which are available for the sum-of-sines signal (designated  $\omega_k$ ):

$$\omega_K = 2\pi \frac{k}{240} \quad (A3)$$

The pitch disturbance  $u$  and the longitudinal disturbance  $x$  were computed as a function of time:

$$u(t) = \sum_{i=1}^{10} a_i \sin(\omega_i t + \rho_i) \quad (A4)$$

$$x(t) = \sum_{j=1}^{10} a_j \sin(\omega_j t + \rho_j) \quad (A5)$$

An initial time was calculated that would make the initial disturbance magnitude equal to zero, minimizing initial transients. For each data run, the phase angles ( $\rho_1, \rho_j$ ) were randomly varied between  $-\pi$  and  $\pi$  (a different value for each frequency). The random number generator used to generate the random angles was seeded with the run number value (from 1 to 8) at the beginning of the run. This ensured that within a particular condition the disturbances would be different on each run (keeping the operator from learning and anticipating the disturbance). It also ensured that the operator would receive the same 8 disturbances in each condition; since the conditions were spaced by at least 30 minutes, and the run lengths were 4 minutes, it is unlikely that the operators were able to detect the repetition of disturbance types over conditions.

pitch disturbance				longitudinal position disturbance			
$i$	$a_i$	$k_i$	$\omega_i$ (rad/sec)	$j$	$a_j$	$k_j$	$\omega_j$ (rad/sec)
1	1.5	5	.131	1	.60	6	.157
2	1.5	8	.209	2	.60	9	.236
3	1.5	13	.340	3	.60	17	.445
4	1.5	23	.602	4	.60	29	.759
5	1.5	37	.969	5	.60	41	1.07
6	.30	59	1.54	6	.30	61	1.60
7	.30	101	2.64	7	.30	103	2.70
8	.15	179	4.69	8	.15	181	4.74
9	.15	311	8.14	9	.15	313	8.19
10	.15	521	13.64	10	.15	523	13.69

**Table A1. Sum-of-sines disturbance characteristics.**

## Acknowledgments

This work was supported by the Human Measures and Performance Project of NASA's Airspace Systems Program (WBS #711-80-03).

## References

- <sup>1</sup>McRuer, D. T., Graham, D., E. Krendel, E., and W. Reisener, Jr., "Human Pilot Dynamics in Compensatory Systems," Air Force Flight Dynamics Laboratory Technical Report: AFFDL-TR-65-15, 1965.
- <sup>2</sup>Kleinman, D. L., Baron, L.S., and Levison, W. H., "An Optimal Control Model of Human Response, Part I," *Automatica*, Vol. 6, No. 3, 1970, pp. 357-369.
- <sup>3</sup>Grunwald, A. J., and Merhav, S. J., "Vehicular Control by Visual Field Cues -- Analytical Model and Experimental Validation," *IEEE Transactions on Systems, Man and Cybernetics*, Vol. 6, No. 12, 1976, pp. 835-845.
- <sup>4</sup>Grunwald, A. J., and Merhav, S. J., "Effectiveness of Basic Display Augmentation in Vehicular Control by Visual Field Cues," *IEEE Transactions on Systems, Man, and Cybernetics*, Vol. 8, No. 9, 1978, pp. 679-690.
- <sup>5</sup>Merhav, S. J., and Grunwald, A. J., "Display Augmentation in Manual Control of Remotely Piloted Vehicles," *Journal of Aircraft*, Vol. 15, No. 3, 1978, pp. 182-189.
- <sup>6</sup>Grunwald, A. J., Robertson, J. B., and Hatfield, J. J., "Experimental Evaluation of a Perspective Tunnel Display for Three-Dimensional Helicopter Approaches," *Journal of Guidance and Control*, Vol. 4, No. 6, 1981, pp. 623-631.
- <sup>7</sup>Grunwald, A. J., "Tunnel Display for Four-Dimensional Fixed-Wing Aircraft Approaches," *Journal of Guidance, Control, and Dynamics*, Vol. 7, No. 3, 1984, pp. 369-377.
- <sup>8</sup>Negrin, M., Grunwald, A. J., and Rosen, A., "Superimposed Perspective Visual Cues for Helicopter Hovering above a Moving Ship Deck," *Journal of Guidance*, Vol. 14, No. 3, 1991, pp. 652-660.
- <sup>9</sup>Grunwald, A. J., and Kohn, S., "Flight-Path Estimation in Passive Low-Altitude Flight by Visual Cues," *Journal of Guidance, Control, and Dynamics*, Vol. 16, No. 2, 1993, pp. 363-370.
- <sup>10</sup>Grunwald, A. J., and S. Kohn, S., "Visual Field Information in Low-Altitude Visual Flight by Line-of-Sight Slaved Helmet-Mounted Displays," *IEEE Transactions on Systems, Man, and Cybernetics*, Vol. 24, No. 1, 1994, pp. 120-134.
- <sup>11</sup>Grunwald, A. J., "Improved Tunnel Display for Curved Trajectory Following: Experimental Evaluation," *Journal of Guidance, Control, and Dynamics*, Vol. 19, No. 2, 1996, pp. 378-384.
- <sup>12</sup>Grunwald, A. J., "Improved Tunnel Display for Curved Trajectory Following: Control Considerations," *Journal of Guidance, Control, and Dynamics*, Vol. 19, No. 2, 1996, pp. 370-377.
- <sup>13</sup>Zacharias, G. L., "Visual Cueing Model for Terrain-Following Applications," *Journal of Guidance, Control, and Dynamics*, Vol. 8, No. 2, 1985, pp. 201-207.
- <sup>14</sup>Zacharias, G. L., "An Estimation/Control Model of Egomotion," *Perception & Control of Self-Motion*, edited by R. Warren and A. H. Wertheim. Lawrence Erlbaum Associates, Hillsdale, 1990, pp. 425-460.
- <sup>15</sup>Baron, S., Lancraft, R., and G. L. Zacharias, G. L., "Pilot/Vehicle Model Analysis of Visual and Motion Cue Requirements in Flight Simulation," NASA CR-3312, 1980.
- <sup>16</sup>Zacharias, G. L., "Modelling the pilot's use of flight simulator visual cues in a terrain-following task," Charles River Analytics, Report No. R8505. Cambridge, MA, 1985.
- <sup>17</sup>Wewerinke, P. H., "The effect of visual information on the manual approach and landing," NLR TR 80055, NLR, 1980.

<sup>18</sup>Wewerinke, P. H., "Visual Scene Perception in Manual Control," *Journal of Cybernetics and Information Science, ASC*, Vol. 3, 1980, pp. 1-4.

<sup>19</sup>Johnson, W., and Phatak A., "Optical Variables and Control Strategy used in a Visual Hover Task," *Proceedings of the IEEE International Conference on Systems, Man and Cybernetics*, Cambridge, MA, 1989. pp. 719-24.

<sup>20</sup>Mulder, M., "Modelling Manual Control of Straight Trajectories with a Perspective Flight-Path Display," *Proceedings of the XVth European Annual Conference on Human Decision Making and Manual Control*, 1996.

<sup>21</sup>Sweet, B. T., "The identification and modeling of visual cue usage in manual control task experiments," Ph.D. Dissertation, Department of Aeronautics and Astronautics, Stanford University, Stanford, CA, 1999.

<sup>22</sup>Sweet, B. T., "The identification and modeling of visual cue usage in manual control task experiments," NASA/TM-1999-208798, 1999.

<sup>23</sup>Sweet, B. T., "A Model of Manual Control with Perspective Scene Viewing", *Journal of Guidance, Control, and Dynamics* (submitted for publication).

<sup>24</sup>Levison, W. H., "Measurement of Human Operator Response Behavior," NASA CR-166038, 1980.

<sup>25</sup>Levison, W. H., "Some Computational Techniques for Estimating Human Operator Describing Functions," *Proceedings of the Twenty-First Annual Conference on Manual Control*, NASA CP 2428, 1986.

<sup>26</sup>Woo, M., Neider, J., Davis, T., and Shreiner, D. *OpenGL Programming Guide*, 3<sup>rd</sup> ed., Addison-Wesley, Reading, 1999, pp. 124, 242-250.

<sup>27</sup>Oving, A. B., and Sweet, B. T., "Visual Cues for Closed-Loop Manual Control of Pitch," TNO-report TM-03-B013, 2003.

<sup>28</sup>Hess, R. A., "A Rationale for Human Operator Pulsive Control Behavior," *Journal of Guidance and Control*, Vol. 2, No. 3, 1979. pp 221-227.